The 8th European Congress on Computational Methods in Applied Sciences and Engineering
ECCOMAS Congress 2022
5-9 June 2022, Oslo, Norway

WEAR MODELLING IN ELASTO-PLASTIC WHEEL-RAIL CONTACT PROBLEMS

ANDRZEJ M. MYŚLIŃSKI[1], ANDRZEJ CHUDZIKIEWICZ[2,3]

[1] Systems Research Institute
ul. Newelska 6, 01-447 Warsaw, Poland
e-mail: myslinsk@ibspan.waw.pl

[2] Warsaw University of Technology
Faculty of Transport
ul. Koszykowa 75, 00-662 Warsaw, Poland
email: ach1@wt.pw.edu.pl

[3] Kazimierz Pulaski University of Technology and Humanities in Radom
Faculty of Transport
ul. Malczewskiego 29, 26-500 Radom, Poland
e-mail: a.chudzikiewicz@uthrad.pl

Key words: Elasto-plastic contact, wear, energy dissipation, semi-smooth Newton method.

Abstract. The paper is concerned with the development of the numerical procedure to solve the wheel-rail contact problem and the computation of the distribution of surface flash temperatures, stresses as well as the wear evolution due to friction. The two-dimensional wheel-rail contact problem between a rigid wheel and an elasto-plastic rail lying on a rigid foundation is considered. The contact phenomenon includes Coulomb friction, frictional heat generation as well as the wear of the contacting surfaces. The displacement and stress of the rail in contact are governed by the coupled elasto-plastic and heat conductive equations. The wear depth function appears as an internal variable in the non-penetration condition updating the gap between the worn surfaces of the bodies. Moreover the dissipated energy due to friction is calculated to evaluate the loss of rail material and to determine the shape of the contacting surfaces during the wear evolution process. This contact problem is solved numerically using the finite element method as well as the operator splitting approach. The plastic flow and friction inequality conditions are reformulated as equality conditions using the nonlinear complementarity functions. The distribution of surface temperatures and stresses as well as the evolution of the shape of the contact surfaces and the wear depth are reported and discussed.

1 INTRODUCTION

Wear is a complex physical process characterized by the deformation and removal of material from a solid surface due to the mechanical action exerted by the another solid [1, 2, 3, 4, 5]. It frequently occurs as a progressive loss of material resulting from the frictional contact interaction of two loaded sliding surfaces. Many different physical and/or chemical factors may generate the occurrence of the wear phenomenon on contacting surfaces. In engineering practice four basic

types of wear are considered: adhesive, abrasive, corrosive and surface-fatigue wear [1]. This wear evolution process is usually slow and depends on the materials and surface properties of the contacting bodies as well as on the contact conditions. Experimental and numerical tests indicate that high temperatures or stress rates may accelerate the wear of structure surfaces [1]. Many attempts have been made to understand the variables influencing the wear phenomenon and to formulate the equations governing it. The techniques to reduce the friction and wear are reviewed in [2]. A comprehensive literature review of wear models and the predictive equations is presented in papers [1, 2, 3].

Many reports indicate [6, 7, 8, 9] that an energy approach to evaluate the wear kinetics provides higher accuracy and stability than Archard model. In energy model the wear volume is proportional to the accumulated dissipated energy by the friction forces and the impact of frictional forces on the wear process through the friction coefficient is more precisely reflected. Using the energy wear coefficient [6] this model relates the wear debris volume and the accumulated dissipated energy.

The wear evolution [10, 11, 12] may have significant impact on the analysis and numerical solution of the contact problem. The material loss in the contact area can generate significant change of its shape and the redistribution of the contact tractions. This in turn may have change the evolution of wear. Therefore the solution of this class of problems is subject of intensive investigation.

In literature the rolling contact problems with heat flow have been considered, among others, in [13, 14, 15]. The thermo-elastic wheel-rail contact is considered in [13] with the coating layer on top of the rail. The mechanical part of the problem is transformed into quasi-static system and numerically solved. The elasto-plastic three-dimensional rolling contact problem with heat flow is modeled in [14] using finite element approach and LS-DYNA software. The elasto-plastic two-dimensional thermo-mechanical rolling contact problem is solved in [15] using semi-smooth Newton method.

This paper deals with the simulation of the wear evolution in elasto-plastic rather than elastic wheel-rail contact problem including Coulomb friction [3] as well as the frictional heat flow [3, 9]. Focusing on wear evolution in wheel-rail elasto-plastic contact problems extends the authors results from [15]. The wheel-rail contact problem is governed by the system of the mildly coupled time-dependent elasto-plastic and conductive equations. The elastic and plastic responses are approximated, respectively, by Hooke's law and by von Mises yield criterion with isotropic power law hardening. The wear phenomenon is modelled using the dissipative energy method where the volume of the worn material governed by the work of the friction force, both in global and local forms. The local form allows to introduce the wear depth function satisfying Archard model. The wear depth function directly enters into the contact non-penetration conditions enforcing the update of a gap between contacting surfaces. The finite element method is used as a discretization method. The associative plastic flow, non-penetration and friction conditions generate inequality type constraints. These conditions are reformulated in an equivalent set of nonlinear complementarity functions and transformed into the set of equality constraints [16]. The coupled nonlinear and non-differentiable system of the equilibrium equations including nonlinear constitutive material behavior and heat flow as well as these equality constraints imposed on nonlinear complementarity functions is solved numerically using semi-smooth Newton method [16]. Since the material removal due to wear may lead to mesh distortion the worn

volume calculated due to dissipated energy method is used to ensure the regularity of the mesh. The distribution of contact stresses and temperatures for elastic and elasto-plastic problems is reported and compared. The obtained numerical results indicate that for the elasto-plastic material model, when the number of cycles is increasing, the plasticity and thermal effects lead to increasing of the contact zone length and the wear depth comparing to the elastic material model.

2 WHEEL - RAIL CONTACT PROBLEM FORMULATION

Consider elasto-plastic deformations of a 2D rail strip lying on a rigid foundation (see Figure 1). The strip has constant height h and occupies domain $\Omega \subset R^2$ with the boundary Γ. A wheel rolls along the upper surface Γ_C of the strip. The wheel has radius r_0, rotating speed ω and linear velocity V. The axis of the wheel is moving along a straight line at a constant altitude h_0 such that $h_0 < h + r_0$, i.e., the wheel is pressed in the strip. It is assumed, that the head and tail ends of the strip are clamped, i.e., the length of the strip is much bigger than the radius of the wheel. Moreover it is assumed, that there is no mass forces in the strip. The body is clamped along a portion Γ_0 of the boundary Γ of the domain Ω. The contact conditions are prescribed on a portion Γ_C of the boundary Γ. The boundaries Γ_0 and Γ_C are disjoint.

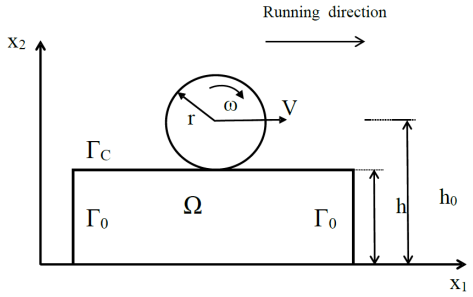

Figure 1: Wheel rolling over the strip.

2.1 Thermo-elasto-plastic model

The thermo-elasto-plastic rolling contact problem is described by the coupled heat conduction and elasto-plastic equations. We will denote by $u = (u_1, u_2)$ a displacement of the strip and by $\theta = \theta(x, t)$ the absolute temperature of the strip. Both the displacement and the temperature are dependent on spatial variable $x = (x_1, x_2) \in \Omega$ and time variable $t \in [0, T]$, $T > 0$. The Cauchy stress and the linearized strain tensor will be denoted [17] by $\sigma = (\sigma_{11}, \sigma_{22}, \sigma_{12})$, where $\sigma_{12} = \sigma_{21}$, and by ε, respectively.

2.1.1 Plasticity model

The small strain plasticity model of strip material is used [17]. In this model the strain $\varepsilon = \varepsilon(u)$ defined as the sum of the displacement gradients is additively decomposed [16] into its

elastic and plastic parts, i.e.,

$$\varepsilon(u) = \varepsilon^e(u) + \varepsilon^p(u), \tag{1}$$

such that the trace of the plastic strain $\varepsilon^p(u)$ is vanishing in the domain Ω. The Cauchy stress tensor $\sigma(u)$ in the domain Ω is the product of the elastic strain $\varepsilon^e(u)$ as well as Hooke's tensor. Under the loading of volume or boundary forces the body material undergoes elasto-plastic deformation with kinematic and isotropic hardening. This deformation with the hardening phenomenon is governed by the generalized plastic strain (ε^p, ξ) and/or the generalized plastic stresses (σ, χ). The back stress χ and the internal variable ξ are related in the domain Ω by

$$\chi = -H\xi, \tag{2}$$

where H denotes a given hardening tensor. The generalized plastic stress may take values only in a set K of admissible generalized stresses. For a given von Mises yield function φ this set is defined as [17]

$$K = \{(\sigma, \chi) : \varphi(\sigma, \chi) \leq 0\}. \tag{3}$$

The evolution of the plastic strain $\varepsilon^p(u)$ and the internal variable ξ is governed by the associative flow rule [9] stating that [17]

$$(d\varepsilon^p, d\xi) = \phi \nabla\varphi(\sigma, \chi) \ \text{ and} \phi \geq 0, \ \ \varphi(\sigma, \chi) \leq 0, \ \ \phi\varphi(\sigma, \chi) = 0, \tag{4}$$

where $d\xi$ denotes the derivative (or increment) of ξ with respect to the time variable and $\nabla\varphi$ is the gradient of the yield function φ.

2.2 Contact model

Denote by ρ and λ as well as by γ a mass density as well as Lamé coefficients [**?**, 16] of the strip material, respectively. Moreover α is a coefficient of thermal expansion and c_p is a heat capacity coefficient. Operator divσ(u) denotes the sum of the first derivatives of the stress function σ with respect to space variable x [17]. Let $\bar{\kappa}$ denotes a thermal conductivity coefficient. By $\triangle\theta$ we denote the Laplacian operator, i.e., the sum of the second order derivatives of function θ with respect to x [17]. For the stress σ satisfying (3)-(4), the displacement u and the temperature θ of the strip satisfy in domain Ω and time interval $(0, T)$ the following system of equations:

$$\rho c_p \frac{\partial^2 u}{\partial t^2} = \text{div} - \alpha(3\lambda + 2\gamma)\nabla\theta \quad \text{and} \quad \rho \mathrm{c_p} \frac{\partial \theta}{\partial \mathrm{t}} = \bar{\kappa} \triangle \theta. \tag{5}$$

The following boundary conditions are imposed: the displacement on the boundary Γ_0 vanishes and the normal stress $\sigma \cdot n$ equals a vector F on the contact boundary Γ_C. Moreover:

$$\bar{\kappa}\frac{\partial \theta}{\partial n} = q \ \text{ on } \ \Gamma_{\mathrm{C}} \quad \text{and} \quad \bar{\kappa}\frac{\partial \theta}{\partial \mathrm{n}} = 0 \ \text{ on } \ \Gamma_0. \tag{6}$$

Function q is given and generally may depend on time and space variables. Here we assume q is constant in time. It depends on the friction coefficient, sliding velocity, tangential force and the thermal resistance coefficient of the strip material. Vector $n = (n_1, n_2)$ denotes outward normal versor to the boundary Γ of the domain Ω. Vector $F = (F_1, F_2)$ is a priori unknown and is given

by the conditions of contact and friction. Under the assumptions that the strip displacement is suitable small [13] the surface non-penetration requirement is governed by the condition on Γ_C:

$$u_2 + g_r + w \leq 0, \quad F_2 \leq 0, \quad (u_2 + g_r + w)F_2 = 0, \tag{7}$$

with $g_r = h - h_0 + \sqrt{r_0^2 - (u_1 + x_1)^2}$ and $w = w(x)$ denoting the gap and the wear depth functions, respectively. The Coulomb friction condition has the form [11]:

$$|F_1| \leq \mu |F_2|, \quad F_1 du_1 \leq 0, \quad (|F_1| - \mu |F_2|)du_1 = 0, \tag{8}$$

where μ is a friction coefficient. Along the boundary Γ_0 the temperature θ is equal to the given temperature θ_g of the surrounding air. At the initial moment $t = 0$ the temperature of rail is assumed to be the same as a given temperature θ_g, i.e., $\theta(x, 0) = \theta_g$ in Ω. For $t = 0$ the displacement $u(x, 0) = 0$.

2.3 Wear evaluation models

Let us introduce a wear law governing the removal of material from the contact interface. We confine to consider abrasive wear where the wear debris are assumed to be expelled from the contact zone. The material removal from the contact zone due to wear can change the shape of the contacting surfaces and lead to the redistribution of contact tractions. On the other hand the update of contact tractions has impact on the wear evolution process. In literature [6, 11] there are two approaches to finite element analysis of contact problems with wear. For the contact problems where the amounts of generated wear is suitable small the shape change of the contact surface due to wear is neglected. The contact problem is solved and next the wear depth rate is calculated and inserted into the non-penetration condition as the wear depth function modifying the normal contact gap between the surfaces. In the second approach the contact zone shape evolution due to the accumulated wear as well as the coupling between the elasto-plastic deformation and wear are taken into account. In this approach first the contact problem is solved and the wear depth is evaluated and next the contact surface is modified. The contact surface update consists in repositioning of the contact nodes in the wear box in order to avoid the distortion of the degenerated finite elements. Therefore to quantify the removal of material from the contacting surfaces due to the friction force we use the dissipated energy method [6].

2.3.1 Dissipated energy method

The dissipated energy method [6] is based on the assumption that the wear volume Vol is proportional to the total dissipated energy E_f due to the friction force, i.e., the following relation holds:

$$Vol = \alpha_f E_f = \alpha_f \sum_i E_{f^i}, \tag{9}$$

where the proportional coefficient α_f called the energy wear coefficient is an independent material parameter [6]. The total dissipated energy E_f is a sum of energies E_{f^i} dissipated in one slip cycle i by the frictional force acting on the contact zone from x_{1min} to x_{1max}. The energy E_{f^i}

is a sum of all contributions of the energy dissipated by the frictional force F_1 moving on the sliding distance from the point x_1 at time $t - \triangle t$ to the point x_1 at time t:

$$E_{f^i} = \int_{t-\triangle t}^{t} \mid F_1 \mid dx_1 = \int_{t-\triangle t}^{t} \mu \mid F_2 \mid dx_1 = \mu \mid F_2 \mid (x_1(t) - x_1(t - \triangle t)), \tag{10}$$

where Coulombs friction law (8) is used and $\triangle t$ denotes a time step. Remark [11] the evolution of the wear phenomenon is obtained using the frictional force and the history of sliding displacement. This feature makes it specially designed for the analysis of contact between solid bodies undergoing plastic strains. The energy wear coefficient may be used [6] for any normal load or displacement amplitude as well as load frequency subject to change during the wear process modeling. System (9)-(10) is called global dissipated energy method [6, 11].

2.3.2 Wear depth evaluation

The local wear analysis [6, 11] implies that the local wear depth distribution w(x) is equal to the product of the total dissipated energy due to friction and the local energy wear coefficient α_w, i.e.

$$w(x) = \alpha_w E_f. \tag{11}$$

Since the change rate of the sliding position can be expressed in terms of the relative tangential velocity du1, taking into account (9)-(10) we obtain that the wear rate function dw is expressed as the product of the local energy wear coefficient, normal contact stress and the relative tangential velocity, i.e.,

$$dw = \alpha_w \mu \mid F_2 \mid du_1. \tag{12}$$

For a unit contact surface $\alpha_w = \alpha_f$ [10]. The wear depth $w(x)$ modifying the gap between the contacting surfaces appears in the non-penetration condition (7). Remark, (12) is equivalent to Archard law of wear. Both (10) and (12) result in the repositioning of the contact nodes at the contact surface and the update of the contact pressure as well as the equilibrium state of the bodies in contact. The considered thermo-elasto-plastic rolling contact problem is governed by (4)-(8), (10)-(12).

3 NUMERICAL SOLUTION METHODS

Since in the system (4)-(8), (10)-(12) the contact traction depends on the thermal distortion of the bodies and on the other hand, the amount of heat generated due to friction depends on the contact traction this system of equations is a coupled thermo-elasto-plastic problem. The main solution strategies for the coupled problems are global solution algorithms where the differential systems for the different variables are solved together or operator splitting methods. In this paper we employ operator split algorithm.

Therefore in the simulation procedure, the elasto-plastic contact and thermal problems are solved sequentially in time. First at time t the elasto-plastic contact problem is solved, i.e., for a given temperature θ at time t the normal contact traction F_2^t and the wear depth w^t are calculated. Next in the thermal analysis step, the heat flux at the consecutive time step $t + \triangle t$ the temperature $\theta^{t+\triangle t}$satisfying the heat equation is calculated. Symbol $\triangle t$ denotes a given time increament. The temperature is calculated for the heat flux approximated by $q^{t+\triangle t} = \mu V F_2^t$.

When two temperatures calculated at times instants t and $t + \triangle t$ differes by a given parameter only the computational process is stopped. If the stop criterion is not satisfied the volume Vol^t of the worn material is calculated using (10)-(12). Based on w^t and Vol^t the average wear depth w_a^t for each surface finite element is calculated. If the aspect ratio for the element is less than the prescribed value the allowed wear depth from the element is removed and the mesh is updated. Next the elasto-plastic contact problem at the time $t + \triangle t$ is solved. Recall in order to calculate the solutions to the problem (1)-(12) we have to regularize it. Let $\epsilon > 0$ be a regularization parameter. We use the following formula [11] relating tangential and normal tractions on the contact boundary Γ_C:

$$F_1 = F_1(\epsilon, F_2, u_1) = -\mu \mid F_2 \mid \arctan(\frac{\mathrm{d}u_1}{\epsilon}). \tag{13}$$

For the methods to solve numerically the mechanical sub-problem see [10, 15]. In finite element formulation a family of nonlinear complementarity matrix functions C_p and C_c applied to plastic yield as well as frictional conditions (4) and (7) combined with the equilibrium equations generates a system of semi-smooth equations. This system is solved using the generalized Newton method. This method can be interpreted as a primal-dual optimization method with the active set strategy [11, 15]. In matrix notation the solution of the mechanical system is equivalent to find at iteration j the solution $(u^j, w^j, (\sigma^j, \chi^j), F_2^j)$ such that

$$Au^j + B_p^j + B_c F_2^j - M_1{}^j = 0, \tag{14}$$

$$w^j = A_w u^j, \tag{15}$$

$$C_p(u^j, w^j, (\sigma^j, \chi^j)) = 0, \tag{16}$$

$$C_c(u^j, w^j, F_2^j) = 0, \tag{17}$$

where $A, A_w, B_c, B_p, M_1, C_p, C_c$ are given finite element matrices [11, 16]. The solution of the thermal system consists in solving the system of linear equations using the Cholesky method. The material removal process due to wear is changing the geometry of the contacting surfaces. At finite element level it leads to the distortion of the mesh. These difficulties are avoided using two step procedure in the form of the wear box [6, 11]. First the weighted wear depth and the deformation of the body are evaluated by solving system (14)-(17). If the wear depth is so large that finite element aspect ratio is not satisfied based on dissipated energy formula (9)-(10) the amount on the worn material is evaluated and the balanced average wear depth value is calculated. The finite elements close to the contact surface are reevaluated and if necessary the worn material is redistributed among these elements.

4 NUMERICAL RESULTS AND DISCUSSION

A series of simulations are conducted in Matlab environment to simulate and to investigate, governed by system (1)-(12) the stress and temperature distributions in the contact area as well as the evolution of worn material and contacting surfaces. The rail strip occupies in Cartesian coordinates 2D domain Ω given by (see Fig. 1):

$$\Omega = \{x = (x_1, x_2) \in R^2 : x_1 \in (-20, 20), x_2 \in (0, 10)\}. \tag{18}$$

Using the finite element method domain Ω has been divided into 1240 quadrilateral 8 nodes elements. The adaptive type of mesh is used to achieve required accuracy of solution, i.e., the finest mesh is in the contact region and the coarse mesh is used far from this area. Numerical data are as follows: the velocity V = 25 m/s, radius of the wheel $r_0 = 0.46$ m, the thermal resistance coefficient r = 1000 KNs/J. The friction coefficient μ is equal to 0.5. The penetration of the wheel is taken as $\delta = 0.1 \cdot 10^{-3}$m, i.e., it is equivalent the action of the force 96 kN. The regularization parameter ϵ in (13) is set to 0.001. The ambient temperature $\theta_g = 20$ deg C.

4.1 Distribution of stresses and temperatures

Figures 2, 3 and 4 display the stresses σ_{22}, σ_{11} and the shear stress σ_{12} on the top surface of the rail (i.e., for $x_2 = 10$) along the x_1-axis for thermo-elasto-plastic material rail model. For the sake of comparison these stresses have been also calculated for elastic and elasto-plastic material rail models and displayed on Figures 2-4. When the contact occurs the stress components are gradually built up. Having reached the maximum value the stress components are decreased as the wheel moves away from the contact zone. The stress σ_{22} attains the highest value for the elastic material model at the middle point of the contact zone. For elasto-plastic and thermo-elasto-plastic material models this stress attains lower values than for pure elastic model. On the other hand the length of the contact zone for elastic-plastic material is higher than for elastic materials. The stress σ_{11} attains the highest value for the thermo-elasto-plastic material. Moreover for these materials the residual stress can also be observed. The shear stress σ_{12} attains the highest value for the elastic material model however this value is significantly lower than peak values for the stresses σ_{22} and σ_{11}.

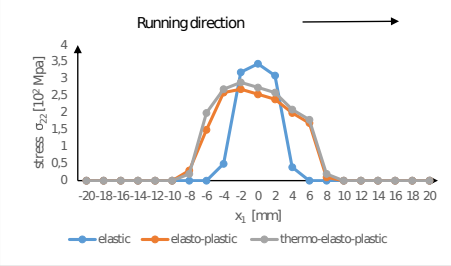

Figure 2: Vertical stress σ_{22} along x_1 axis on the rail top surface.

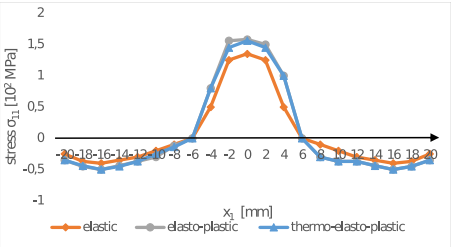

Figure 3: Longitudinal stress σ_{11} along x_1 axis on the rail top surface.

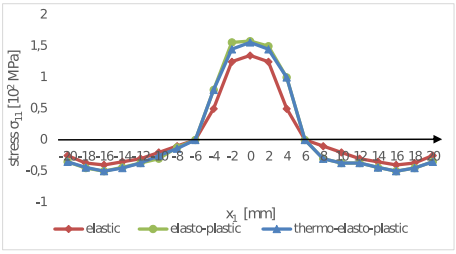

Figure 4: Shear stress σ_{12} along x_1 axis on the rail top surface.

In order to compare the impact of plasticity or thermal effects on these stresses the equivalent von Mises stress has been calculated for these material models. Figures 5 and 6 display the distribution of von Mises stress along the x_1 axis on the top of the rail surface (i.e., for $x_2 = 10$) as well as maximal values of this stress for different material rail models. It results that for the elastic material model the peak stress appear almost in the middle of the contact zone. In case of both elasto-plastic materials this peak stress is moved slightly forward in running direction towards the leading edge of the contact zone. It occurs at a point where the maximum plastic deformation appears due to the hardening and conformity increase between the contacting surfaces. The peak stress for the elastic model is higher than for both elasto-plastic material rail models. Comparing thermal-elasto-plastic and elasto-plastic models it can be seen that the peak stress for thermo-elasto-plastic material model is slightly higher than this peak for elasto-plastic material models. Thermal effects in the plastic range lead to the increase of the stress. For the wheel far enough from the localization of peak stress point the strain vanishes for the elastic material model. In material model with plasticity after the loading there are non-vanishing plastic strains, slightly higher for material with thermal effects. These observations can be summarized in the following way:

- the plasticity results in decreasing of the peak stress comparing to elastic case due to the work of plastic deformation,
- thermal effects leads to increase of the peak stress for elasto-plastic materials rail models.

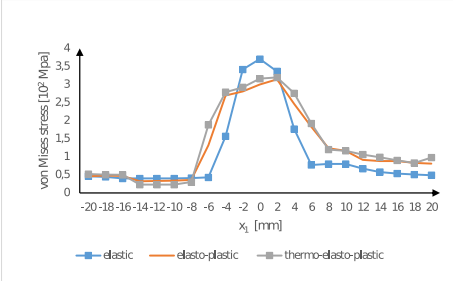

Figure 5: Von Mises stress along x_1 axis on the rail top surface.

Figures 7 and 8 display the temperature distribution along the x_1 axis and x_2 axis, respectively. The temperature for both thermo-elastic and thermo-elasto-plastic materials rapidly

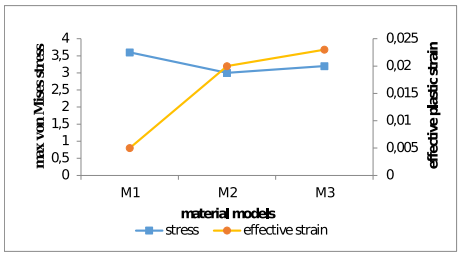

Figure 6: Maximal values of von Mises stress as well as effective plastic strain for different materials (M1: elastic, M2: elasto-plastic, M3: thermo-elasto-plastic.

increases in the contact zone. It attains maximum in the center of this region and rapidly decays in front of the moving wheel. The peak rail temperature for elastic material model is equal to 210 degree C and is higher than the peak temperature 150 degree C for the elasto-plastic model. Remark for nonlinear material model the lower tangential contact stress occurs. Moreover for these models a part of the total energy is used to form plastic deformation. Hence it results in lower peak temperatures for elasto-plastic materials models. Remark also [12] temperature simulation results are also strongly dependent on such data as friction coefficient, linear velocity and mass of the wheel. Higher values of these parameters results in higher peak temperatures on the rail surface.

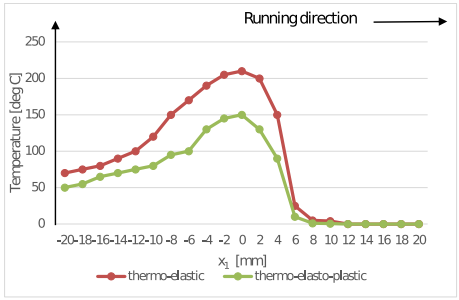

Figure 7: Longitudinal temperature distribution along x_1 axis.

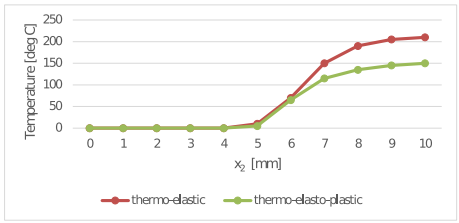

Figure 8: Vertical temperature distribution along x_2 axis.

Figures 9 and 10 display for this example the fretting wear surface evolution for three different set of cycles where the displacement amplitude along the x_1 axis equals $\delta x = 75 \cdot 10^{-6}$ m. The

plasticity effect results in increasing of the contact zone as well as the wear depth as the number of cycles is increasing. Moreover as the number of cycles is increasing due to temperature field the length of contact zone as well as the wear depth are also increasing.

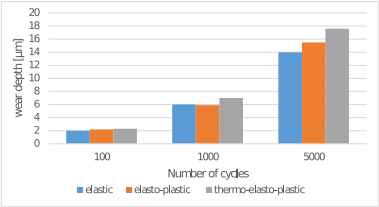

Figure 9: The wear depth evolution depending on the number of cycles.

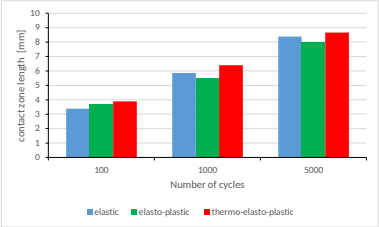

Figure 10: The length of the contact zone evolution depending on the number of cycles.

5 CONCLUSIONS

The dissipated energy method and contact interface shape update strategy are efficient and precise tools to evaluate the wear distribution. The impact of hardening parameters as well as temperature dependent material parameters and creepage on the wear evolution process requires further research. The wear evolution process where the location of contact zone may be also treated as the shape optimization problem [18]. Therefore the choice of parameters ensuring the minimization of the worn material volume may be considered and formulated as the shape optimization problem where the dissipated energy is the criterion of optimization.

REFERENCES

[1] Meng, H.C. and Ludema, K.C. Wear models and predictive equations: their form and content. *Wear* (1995) **181-183**:443-457.

[2] Harmon, M. and Lewis, R. Review of top of rail friction modifier tribology. *Tribology: Materials, Surfaces and Interfaces* (2016) **10**(3):150-162.

[3] Vakis, A.I., et al. Modeling and simulation in tribology across scales: An overview. *Tribology International* (2018) **125**:169-199.

[4] Al-Maliki, H., Meierhofer, A., Trummer, G., Lewis, R., Six, K. A new approach for modelling mild and severe wear in wheel-rail contacts. *Wear* (2021) **476**:203761.

[5] Li, J., Zhou, Y., Lu, Z., Wang, Z., Cheng, Z., Wang, S. Experimental study on the mechanism of wheel-rail steels crack initiation and wear growth under rolling contact fatigue. *Procedia Structural Integrity* (2022) **37**:582-589.

[6] Fouvry, S., Paulin, C., Liskiewicz, T. Application of an energy wear approach to quantify fretting contact durability. Introduction to wear energy capacity concept, *Tribology International* (2007) **40**:1428-1440.

[7] Jahangiria, M., Hashempourb, M., Razavizadehb, H., Rezaieb, H.R. A new method to investigate the sliding wear behaviour of materials based on energy dissipation: W25 wt% Cu composite. *Wear* (2012) **274/275**:175-182.

[8] Abdo, J. Materials Sliding Wear Model Based on Energy Dissipation. *Journal of Mechanics of Advanced Materials and Structures* (2015) **22**(4):298-304.

[9] Alarcon, G.I., Burgelman, N., Meza, J. M., Toro, A., Li, Z. Power dissipation modeling in wheel/rail contact: Effect of friction coefficient and profile quality. *Wear* (2016) **366-367**: 217-224.

[10] Braghin, F., Lewis, R., Dwyer-Joyce, R.S., Bruni, S. A mathematical model to predict railway wheel profile evolution due to wear. *Wear* (2006) **261**:1253 1264.

[11] Doca, T., Andrade Pires, F.M. Finite Element Modelling of Wear using the Dissipated Energy Method coupled with a Dual Mortar Contact Formulation. *Computers and Structures* (2017) **191**:62-79.

[12] Fouvry, S., Paulin, C. An effective friction energy density approach to predict solid lubricant friction endurance: Application to fretting wear. *Wear* (2014) **319**:211-226.

[13] Chudzikiewicz, A., Myśliński, A. Thermoelastic Wheel-Rail Contact Problem with Elastic Graded Materials. *Wear* (2011) **271**:417-425.

[14] Naeimi, M., Li, S., Li, Z., Wu, J., Petrov, R., Sietsma, J., Dollevoet, R. Thermomechanical analysis of the wheel-rail contact using a coupled modelling procedure. *Tribology International* (2018) **117**:250-260.

[15] Myśliński, A. and Chudzikiewicz, A. Wear modelling in wheel-rail contact problems based on energy dissipation. *Tribology - Materials, Surfaces and Interfaces* (2021) **15**:138-149.

[16] Hager, C., Wohlmuth, B. I. Nonlinear complementarity functions for plasticity problems with frictional contact. *Comput. Methods Appl. Mech. Engrg.* (2009) **198**:3411-3427.

[17] Han, W., Reddy, B.D. *Plasticity. Mathematical Theory and Numerical Analysis*, 2nd edition, New York, Springer (2013).

[18] Myśliński, A., Wróblewski, M. Structural optimization of contact problems using Cahn-Hilliard model. *Computers and Structures* (2017) **180**:52-59.